chemengineering

MDPI

Article

Optimizing Photocatalytic Lead Removal from Wastewater Using ZnO/ZrO_2: A Response Surface Methodology Approach

Hiba Abduladheem Shakir, May Ali Alsaffar *, Alyaa K. Mageed, Khalid A. Sukkar and Mohamed A. Abdel Ghany

Department of Chemical Engineering, University of Technology-Iraq, Baghdad 10066, Iraq; hiba.a.shakir@uotechnology.edu.iq (H.A.S.); alyaa.k.mageed@uotechnology.edu.my (A.K.M.); khalid.a.sukkar@uotechnology.edu.iq (K.A.S.); mohammed.a.abdelghany@uotechnology.edu.iq (M.A.A.G.)
* Correspondence: may.a.muslim@uotechnology.edu.iq or mayrashid1973@gmail.com

Abstract: One interesting method for environmental remediation is the use of ZnO/ZrO_2 composites in the photocatalytic degradation of lead (Pb) in wastewater. Several studies have investigated different types of composites for the removal of heavy metals from wastewater. However, the efficiency of these composites in removing the heavy metals remains debatable. Hence, this study investigated the potential of using a ZnO/ZrO_2 composite for the removal of Pb from wastewater. Response surface methodology (RSM) was utilized in this work to maximize the Pb photocatalytic removal over ZnO/ZrO_2 in simulated wastewater. Based on a central composite design (CCD), the experimental design included adjusting critical process parameters such as catalyst dosage, initial Pb concentration, and pH. The ZnO/ZrO_2 composite was synthesized using a physical mixing technique, and its physicochemical properties were studied by field emission scanning electron microscopy (FESEM), energy dispersive X-ray spectroscopy (EDS), Fourier transform infra-red (FTIR), and X-ray diffraction (XRD). Under visible light irradiation, photocatalytic Pb removal tests were carried out in a batch reactor. The findings showed that a ZnO/ZrO_2 dose of 100 mg/L, a pH of 10, and an initial Pb content of 15 ppm were the optimal conditions for maximal Pb removal (above 91.2%). The actual Pb removal obtained from the experimental runs was highly correlated with that predicted using the RSM quadratic model. The usefulness of ZnO/ZrO_2 composites for photocatalytic Pb removal is demonstrated in this work, which also emphasizes the significance of RSM in process parameter optimization for improved pollutant degradation. The models that have been proposed offer significant perspectives for the development and scalability of effective photocatalytic systems intended to remove heavy metals from wastewater.

Keywords: photocatalytic wastewater treatment; ZnO/ZrO_2 nanocomposite; central composite design; lead degradation

Citation: Shakir, H.A.; Alsaffar, M.A.; Mageed, A.K.; Sukkar, K.A.; Ghany, M.A.A. Optimizing Photocatalytic Lead Removal from Wastewater Using ZnO/ZrO_2: A Response Surface Methodology Approach. *ChemEngineering* **2024**, *8*, 72. https://doi.org/10.3390/chemengineering8040072

Academic Editor: Ori Lahav

Received: 22 May 2024
Revised: 30 June 2024
Accepted: 8 July 2024
Published: 11 July 2024

1. Introduction

The presence of high levels of heavy metals in wastewater is a significant environmental issue since it may have detrimental impacts on ecosystems and human health [1–3]. Amongst the recalcitrant heavy metals that has been investigated, lead (Pb) has been reported to be very dangerous and long-lasting in the environment [4,5]. It is a hazardous heavy metal that presents significant health dangers and is difficult to eliminate using traditional techniques [6]. Conventional techniques for removing Pb from wastewater, such as precipitation, filtering, and adsorption, frequently suffer from drawbacks in terms of performance and cost efficiency [7–9]. Photocatalysis has become a highly promising technique for breaking down and eliminating a wide range of contaminants from water [10,11]. The utilization of photocatalysis for the degradation of heavy metals in wastewater has garnered considerable interest owing to its capacity for effective and environmentally friendly water treatment [12,13]. Hojjati-Najafabadi et al. [14] reported the use of cadmium sulfide as photocatalyst for the degradation of methyl blue. The results revealed that the

photocatalyst was effective in the methyl blue degradation at optimum conditions. More precisely, employing semiconductor photocatalysts while exposing them to light provides a sustainable and effective method for eliminating heavy metals such as Pb [15]. Zinc oxide (ZnO) and zirconium dioxide (ZrO_2) are semiconductor materials that are well-known for their capacity to catalyze chemical reactions using light and their ability to remain stable even in extreme environments [16–19]. These photocatalysts have shown great potential in removing Pb through the process of photocatalysis [20–22]. ZnO is recognized for its potent oxidizing ability and large energy gap, while ZrO_2 demonstrates durability and resistance to corrosion, rendering them appropriate choices for environmental cleanup purposes [23–25]. The composite form of ZnO and ZrO_2 has demonstrated superior photocatalytic activity as compared to their separate forms [26]. The increased activity is due to the synergistic effects of the two materials, which result in greater separation of charges and a wider spectrum of light absorption [27]. This leads to higher efficiency in degrading pollutants.

Optimizing process parameters using statistical methods such as response surface methodology (RSM) can greatly boost the efficacy of a photocatalyst [28]. RSM enables a methodical investigation of the relationships between important process variables in order to obtain the most favorable circumstances for the highest possible elimination of pollutants [29]. RSM is commonly used to improve photocatalytic processes for the removal of heavy metals [30,31]. The RSM optimization approach allows for a methodical investigation of crucial process variables, including catalyst dose, initial Pb (ion) concentration, and pH. Researchers have successfully developed mathematical models that can predict the best conditions for the maximal removal of Pb using different photocatalysts [32]. This has been achieved by systematically changing the process parameters in specified experimental designs. Nevertheless, there are still deficiencies in the existing literature when it comes to fully optimizing ZnO/ZrO_2 photocatalysts for the removal of Pb utilizing RSM. Additional research is required to investigate the relationships between process variables and to confirm the efficiency of the optimized conditions in wastewater treatment scenarios.

This study therefore focused on examining the process of removing Pb from wastewater through the use of a ZnO/ZrO_2 composite using a photocatalytic approach. The objective was to optimize the operational parameters such as the dosage of catalyst used, the initial concentration of Pb, and the wastewater pH in order to achieve the highest possible efficiency in removing the Pb. By employing RSM, we could effectively simulate and forecast the correlation between these factors and the response (Pb removal %), thereby simplifying the determination of the most favorable process parameters. This research is important because it enhances our comprehension of the photocatalytic processes used for eliminating heavy metals and offers crucial knowledge for creating effective and environmentally friendly wastewater treatment systems.

2. Materials and Methods

2.1. Material

In this work, analytical grade materials were used. The precursors consisted of HCl and NaOH with concentrations of 99%, lead (II) nitrate, zirconium oxide, and zirconium hydrate. For pH adjustment, analytical research-grade (99.9%) NaOH and HCl were utilized. The reagents were all of the highest purity and analytical grade. The entire experiment was conducted using distilled water.

2.2. Preparation of the Simulated Pb Contaminated Wastewater

To prepare the simulated water, lead (II) nitrate was dissolved in de-ionized water to form a specified concentration of Pb (ions) in ppm [33].

2.3. Preparation Composite

A nano-composite composed of Zinc oxide and zirconium dioxide was prepared by mixing the powders in a weight ratio of 50:50 [34]. The zinc oxide and zirconium dioxide

were mixed by grinding the powders in a mortar with a pestle for approximately 15 min to ensure the homogeneity of the mixture. Subsequently, in order to further ensure the homogeneity, the mixture was placed in a mechanical shaker for 2 h and stored in an Eppendorf tube for further characterization and its application in photocatalysis.

2.4. Batch Experimental Setup of the Photocatalytic Process

A cylindrical Pyrex® glass reactor with a working capacity of 0.25 L and dimensions of 9 cm in height and 7.5 cm in its inner diameter was used to conduct the photocatalytic process. A UV light lamp (8 W, 0.7 w/m^2, and 254 mm wavelength) was used as the light source. The adsorption–desorption equilibrium was confirmed by stirring the ZnO-ZrO_2 mixture with 0.1 L of the simulated Pb wastewater in the reactor at 350 rpm for 15 min in the dark. The initial Pb concentration in the wastewater varied from 40–150 ppm. The dosages of ZnO-ZrO_2 varied from 100–500 mg to determine their effects on the Pb removal from the wastewater. The pH of the simulated wastewater varied from 4–10. The temperature of the reaction was maintained at 25 °C. After that, the reactor was left in direct sunlight for 2 h to initiate the photocatalytic reaction. The wastewater sample was subsequently withdrawn from the glass reactor and filtered using nano-filter paper. The heavy water concentration was determined using atomic absorption spectroscopy. The percentage removal of the Pb (ions) from the simulated water was calculated using Equation (1), as follows:

$$\%\mathrm{Pb(ion|\ )removal} = \frac{C_o - C}{C_o} \times 100, \quad (1)$$

where C_o and C depict the initial and final concentrations of Pb^{+2}, respectively.

2.5. Optimization by Response Surface Methodology (RSM)

The effects of factors such as pH, initial concentration of the Pb in the wastewater, and ZnO/ZrO_2 dosage on the Pb (ion) removal from the wastewater was investigated using a central composite experimental design [32]. The detail of the design is depicted in Table 1. The RSM methodology was then used to optimize the various parameters. This method models experimental data using an appropriate polynomial equation. In order to optimize the values of various factors to obtain the optimal system performance, the RSM approach is suitable for concurrently examining the influence of several variables on a set of responses [35]. The factors used in this study were chosen based on the findings from the literature that have reported their influence on Pb removal from wastewater.

Table 1. Summary of the factors and levels used in the CCD.

Factor	Low	High
pH	4	10
Initial concentration (ppm)	4	15
ZnO/ZrO_2 dosage (mg)	100	500

2.6. Characterization of the ZnO/ZrO_2 Photocatalyst

The materials' crystal structures and characteristics were determined using an X-ray powder diffraction analyzer (XRD) (Shimadzu-6000, Kyoto, Japan). The morphology of the ZnO, ZrO_2, and ZnO/ZrO_2 samples were examined using field-emission scanning electron microscopy (FESEM) (MIRA3, TESCAN, Brno, Czech Republic). Energy dispersive X-ray spectroscopy (EDS) coupled with the FESEM was used to determine the chemical composition of the ZnO, ZrO_2, and ZnO/ZrO_2. Additionally, the textural properties of the photocatalysts were measured using N_2 physisorption analysis, where a Brunauer–Emmett–Teller (BET) device (Q-surf 9600, HORIBA Instruments Inc., Piscataway, NJ, USA) was adopted to measure the specific surface area. The Fourier-transform infrared (FTIR) spectra of the sample were obtained to determine their functional groups using a spectrometer (IRAffinity-1-1900, Shimadzu, Kyoto, Japan) with a 390–4000 cm^{-1}

spectrum. Photoluminescence spectra were recorded using a spectrometer (Perkin Elmer LS55). The Kubelka–Munk theory, represented in Equation (2), was employed to determine the optical band gaps. In this equation, h represents the Planck constant, α denotes the light absorption coefficient, v represents the radiation frequency, and k signifies a parameter that depends on the probability of transition. The Tauc plot was utilized in the current scenario, yielding a value of 1 for n [36]. Thus, the calculated band gap for the ZnO/ZrO_2 sample was determined to be direct.

$$\alpha(hv) = k\left(hv - E_g\right)^{1/n}. \quad (2)$$

3. Results and Discussion

3.1. Characterization of the ZnO, ZrO_2, and ZnO/ZrO_2

The FTIR spectroscopy spectra of the ZnO, ZrO_2, and $ZnO\text{-}ZrO_2$ nanoparticles in their pure forms are depicted in Figure 1. The spectra of all the nanomaterials materials exhibited peaks in a wavenumber range of approximately 390 cm^{-1} to 500 cm^{-1}, indicating the presence of metal–oxygen bonding between the Zn and O, as well as between the Zr and O [37]. The peaks seen at approximately 3460 cm^{-1} and 1500 cm^{-1} in all samples corresponded to the vibrational bands of the hydroxyl groups (O-H) adsorbed on the surface [38]. These peaks represented the stretching and bending motions of the hydroxyl groups. The presence of hydroxyl groups in the produced compounds was clear evidence since they had not undergone calcination. Also, it is important to acknowledge that these interactions were more prominent in samples containing ZrO_2 due to the amorphous characteristics of these products and the creation of bonds between the O and H and the Zr and O [39]. The bands, specifically at 1022 cm^{-1} and 758 cm^{-1}, emerged following the modification of ZnO with ZrO_2. The presence of bands at 688 cm^{-1} and 1022 cm^{-1} indicated the occurrence of Zn-O-Zr stretching vibrations. Additionally, the band at 1402 cm^{-1} suggested the presence of an OAH group in the molecule on the surface. The intense peaks seen in the range of 1360–1420 cm^{-1} were attributed to carbonate anions, which were present due to the utilization of sodium carbonate as a precipitating agent [39].

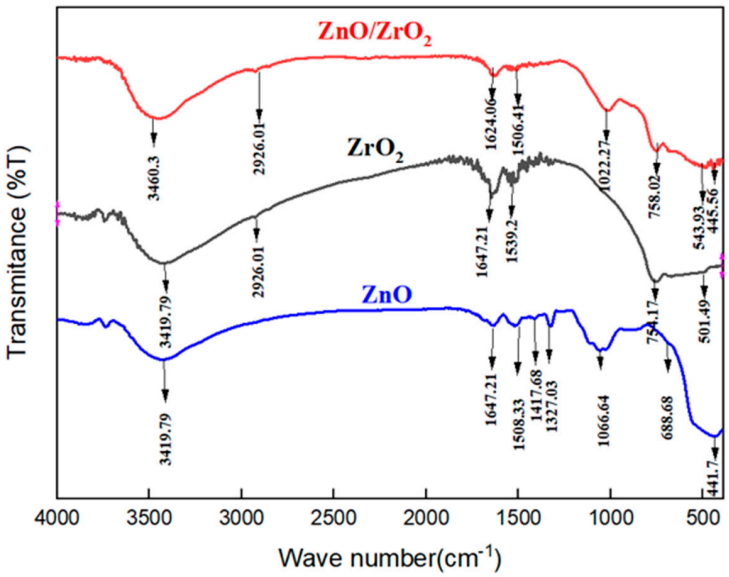

Figure 1. FTIR spectrum of the ZnO, ZrO_2, and$ZnO\text{-}ZrO_2$.

The XRD patterns of the ZnO, ZrO_2, and ZnO/ZrO_2 are depicted in Figure 2. Sharp peaks attributed to ZnO can be observed at 2θs of 31.75°, 34.40°, 36.24°, and 47.54° and 56.61°, 63.13°, and 69.188°, and these correspond to (100), (002), (101), (012), (110), (432), and (343), respectively. The prepared crystalline ZnO's XRD pattern was consistent with the hexagonal zincate crystalline structure of ZnO [40]. The distinctive planes at 2θs of 23.88°, 27.9°, 31.28°, 34.039°, 40.438°, 49.9°, 53.988°, 55.188°, 59.8°, 62.68°, 65.538°, and 71.138° were

verified by the XRD patterns for pure ZrO_2 [41]. These corresponded to (102), (121), (004), (300), (320), (240), (240), (151), (125), (440), and (610), respectively. As depicted in Figure 2, the ZnO-ZrO2's XRD patterns showed distinctive peaks at 2θ = 24.09°, 28.25°, 31.66°, 34.343°, 36.043°, 40.85°, 47.64°, 49.238°, 56.44°, 59.89°, 62.89°, and 68.19°, respectively [42]. These peaks corresponded to the Miller indices (100), (010), (101), (110), (011), (200), (020), (102), (211), (112), and (202), respectively. This suggested that the ZnO-ZrO_2 was nanosized and well-crystallized, confirming its monoclinic phase [43]. The matching peaks for ZnO and ZrO_2 were present in the ZrO_2-ZnO, and the peaks remained strong and sharp. Furthermore, compared to pure ZnO and ZrO_2, the diffractograms depicting ZnO–ZrO_2 exhibited homogenous patterns, indicating a higher amount of amorphous structure [44]. The patterns implied that the materials' surface was more polydisperse, which improved its photocatalytic qualities. The crystalline sizes of the ZnO-ZrO_2 nanoparticles (D) were evaluated according to the Debye–Scherrer equation (Equation (3)) [45]. Zinc oxide-zirconia dioxide nanoparticles have been reported to have a particle size of 22.19 nm.

$$D = \frac{K\lambda}{\beta Cos\theta}, \tag{3}$$

where K is the Scherrer constant, λ is the X-ray wavelength, β is the peak width of the half-maximum, and θ is the Bragg diffraction angle.

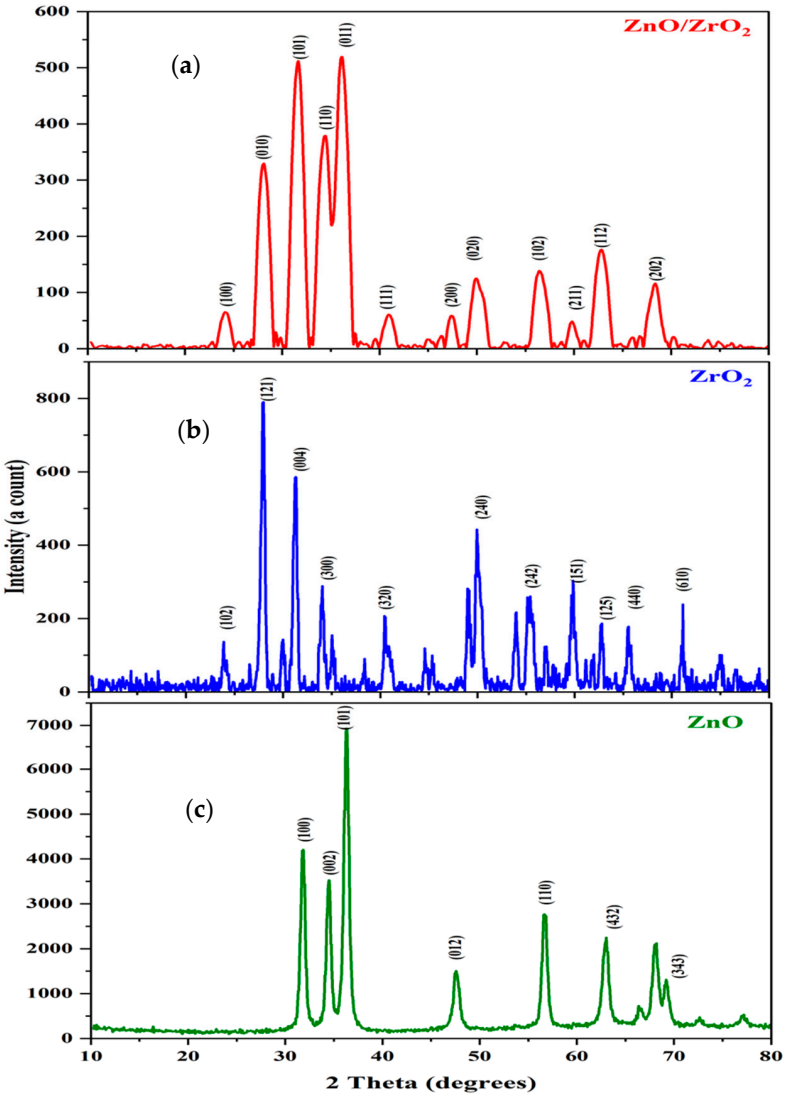

Figure 2. XRD patterns of the (**a**) ZnO/ZrO_2, (**b**) ZrO2, and (**c**) ZnO.

3.2. FESEM and EDS Analysis

FESEM micrographs were used to examine the ZnO/ZrO_2 nanoparticles' morphologies. The precise morphologies of the nanoparticles were examined by taking FESEM micrographs at different magnifications, as seen in Figure 3. The agglomerated nanoparticles' formation was confirmed by the surface morphology. Agglomeration in ZnO/ZrO_2 photocatalysts can arise from several sources, and it is often associated with the intrinsic characteristics of the nanoparticles and the circumstances of their synthesis. Nanoparticles may agglomerate when subjected to mechanical stresses during synthesis of a photocatalyst. Further, ZnO and ZrO_2 nanoparticles exhibit elevated surface energies as a result of their diminutive dimensions and expansive surface areas, and the nanoparticles are compelled to limit their surface areas by agglomerating due to their high surface energies, resulting in a reduction in the overall energy of the system. Figure 3a–c shows the FESEM micrographs of the nanoparticles taken at three distinct magnifications. The pictures revealed aggregated, irregular, and quasi-spherical particles. All three cases shown in Figure 3a–c had the same agglomerated particles and uneven forms [44].

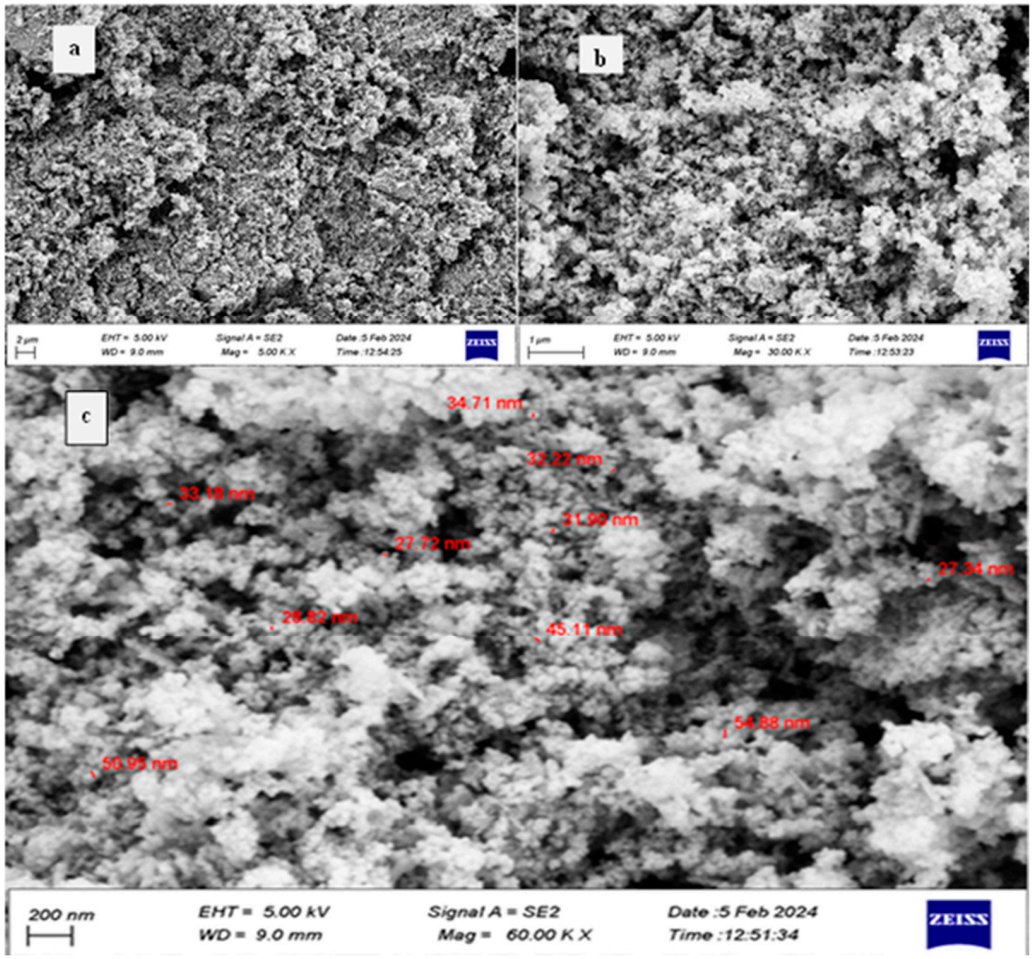

Figure 3. FESEM micrographs of (**a**) 5 KX, (**b**) 30 KX, and (**c**) 60 KX of the ZnO/ZrO_2 nanoparticles.

As demonstrated in Figure 4a–c, an EDS analysis was also performed to validate the resultant composite's elemental makeup. The existence of ZnO and ZrO_2 was shown by the strong peaks from the Zn, Zr, and O_2. The relative intensities of the various peaks could offer qualitative insights into the amounts of ZnO and ZrO_2. As a result of its homogeneity, the percentages of the material's composition ranged from 33.94 %wt. to 38.16 %wt. depending on the sample's examination location.

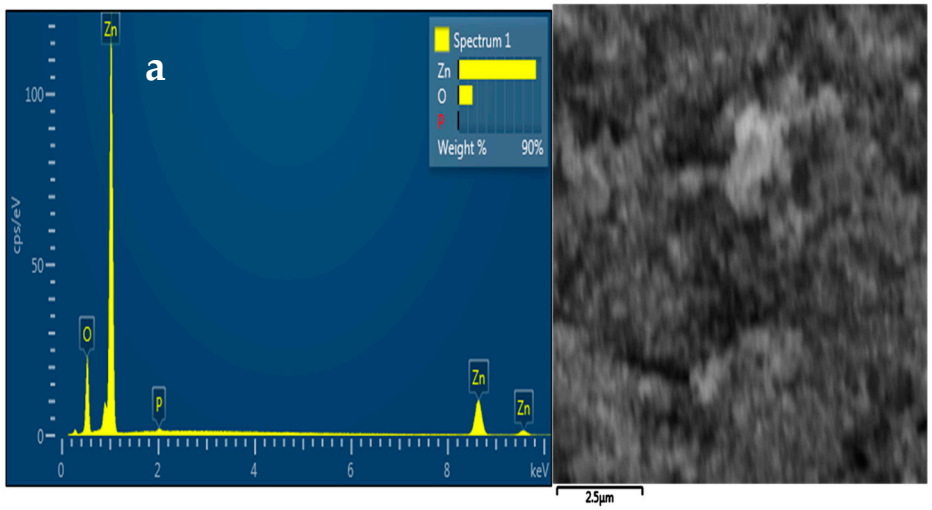

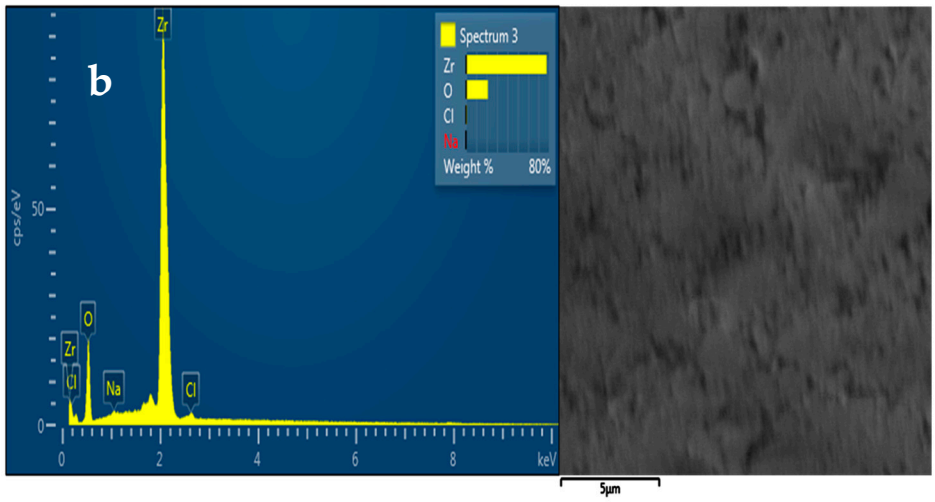

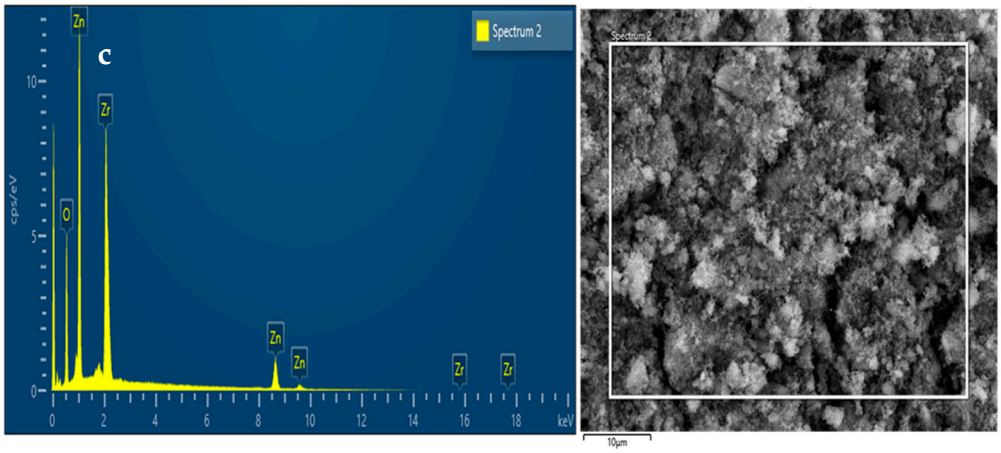

Spectrum 2				
Element	Line Type	Weight %	Weight % Sigma	Atomic %
O	K series	27.90	0.36	64.59
Zn	L series	38.16	0.33	21.62
Zr	L series	33.94	0.37	13.78
Total		100.00		100.00

Figure 4. EDS micrographs of the (**a**) ZnO, (**b**) ZrO_2, and (**c**) ZnO/ZrO_2 nanoparticles.

3.3. Energy Band Gap

The band gap energy and UV-vis spectrum of ZnO-ZrO_2 are shown in Figure 5. According to Figure 5a, the sample had an absorption boundary at approximately 375 nm [38]. Figure 5b was used to graphically determine the band gap energy. The energy band gap

that was achieved for the ZnO-ZrO_2 was 3 eV, as shown in Figure 5b. To improve its photocatalytic activity, a material with a small band gap may be stimulated by solar light more easily, leading to the generation of photogenerated electrons and holes.

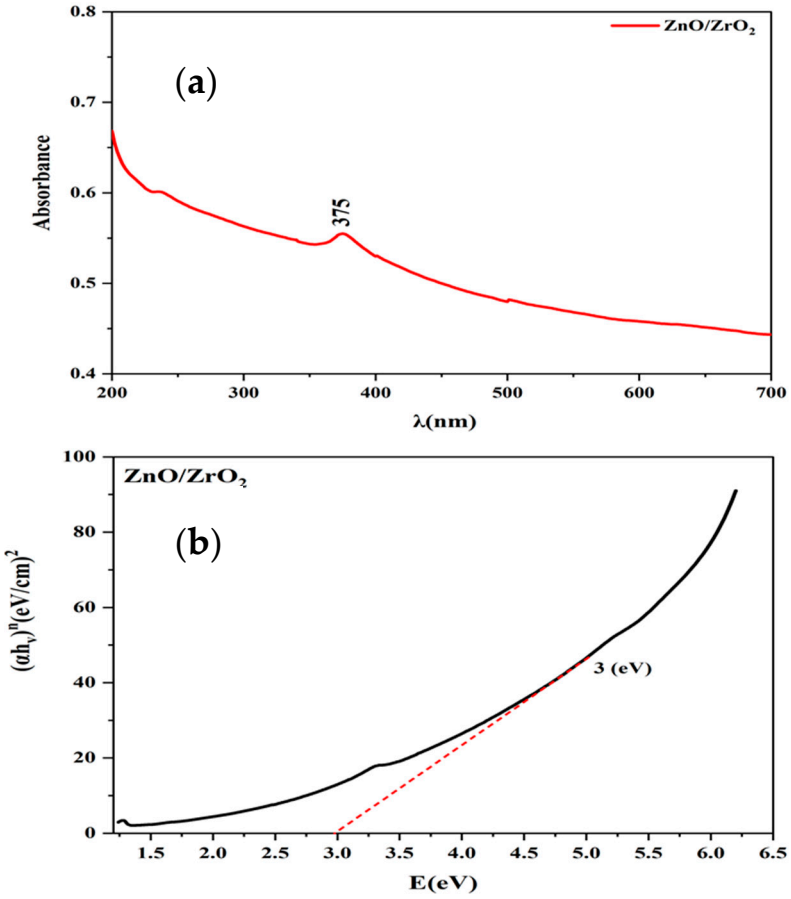

Figure 5. (**a**) UV-vis and (**b**) energy band gap analysis of the ZnO/ZrO_2 nanoparticles.

3.4. Response Surface Optimization

The effects of factors such as the pH, initial ion concentration, and dosage of the ZnO/ZrO_2 photocatalysts in the simulated wastewater on the Pb removal as designed using CCD are summarized in Table 2. As shown in Table 1, the treatment combination of the factors yielded corresponding responses (Pb removal).

Table 2. Summary of the factors and the corresponding responses obtained from the CCD experiment.

Run	A:pH	B: Initial Ion Conc	C:Dosage	Pb Removal
		(ppm)	mg	%
1	4	4	500	63.45
2	7	9.5	100	72.34
3	1.84344	9.5	300	36.23
4	10	4	100	82.12
5	4	4	100	55.34
6	10	15	500	88.21
7	10	4	100	83.23
8	7	9.5	300	75.23
9	7	9.5	643.77	86.23
10	7	9.5	300	71.13
11	7	9.5	300	73.13
12	7	9.5	300	74.21

Table 2. *Cont.*

Run	A:pH	B: Initial Ion Conc	C:Dosage	Pb Removal
13	10	15	100	94.23
14	7	9.5	300	76.32
15	7	18.9537	300	75.23
16	4	15	500	52.23
17	4	4	500	65.35
18	7	9.5	300	78.23
19	10	15	100	86.21
20	10	15	500	83.24
21	7	9.5	300	77.23
22	12.1566	9.5	300	80.12
23	4	4	100	57.45
24	7	0.046316	300	70.23
25	10	4	500	84.23
26	4	15	100	63.26
27	10	4	500	84.13
28	7	9.5	300	77.23
29	4	15	100	60.23
30	4	15	500	51.22

The analysis of variance (ANOVA) showing the significance of the individual, the interaction, and the quadratic effects on the response surface quadratic models is summarized in Table 3. It can be seen that the pH and the initial Pb (ion) concentration had significant interaction effects on the Pb removal from the wastewater, as represented by the *p*-value (<0.05). However, the dosage of the ZnO/ZrO_2 was not statistically significant, as indicated by a *p*-value of >0.05. Also, the interactions between the factors were analyzed. The analysis revealed that the interaction between the pH and initial Pb concentration as well as the interaction between the initial Pb ion concentration and the ZnO/ZrO_2 dosage were statistically significant, as indicated by the *p*-values of <0.05. However, the interaction between the pH of the simulated wastewater and the catalyst dosage was not statistically significant since the *p*-value was >0.05. Furthermore, the quadratic effects of the pH and the catalyst dosage on the simulated wastewater were significant since the *p*-values were <0.05, whereas the quadratic effect of the initial ion concentration was not significant since the *p*-value was >0.05. In summary, the modeled F-value of 57.05 indicated that the model was statistically significant. The probability of an F-value of this magnitude occurring only due to noise was extremely low (0.01%). The *p*-values below 0.0500 implied that the model terms were statistically significant. The main model terms in this example included A, AB, BC, A^2, and C^2. The values over 0.1000 implied that the model terms were not statistically significant. If a model has several irrelevant model terms, except those necessary for hierarchy, then model reduction can enhance such a model. The lack-of-fit F-value of 2.87 indicated that there was a 5.16% probability that a lack-of-fit F-value of this magnitude may have arisen from random variation. Inadequate conformity is undesirable, and the fact that this chance was quite low—less than 10%—was concerning.

The three-dimensional plots showing the interactions between the factors and the Pb removal from the simulated wastewater are depicted in Figure 6. In Figure 6a, it can be seen that a gradual increase in the pH from 4 to 10 resulted in a corresponding increase in the Pb ion removal from the wastewater. This implied that that high concentrations of Pb removal from the wastewater were favored at a pH of 10. However, there was a slight increase in the Pb removal from the wastewater as the catalyst dosage increased. A similar interaction between the pH and the catalyst dosage can also be observed in Figure 6b. However, as shown in Figure 6c, there was not much influence of the interaction between the initial Pb concentration and the catalyst dosage on the Pb removal. The F-statistic of the three-dimensional fittings of the experimental data revealed that the R^2, adjusted R^2, and predicted R^2 were calculated as 0.9625, 0.9456, and 0.9160, respectively. The difference

between the two values was less than 0.2, suggesting that the adjusted R^2 value of 0.9456 and the predicted R^2 value of 0.9160 were reasonably close. The response surface quadratic equation, when expressed in terms of actual factors, is depicted in Equation (4). It allows for making precise predictions regarding the reaction for specific amounts of each element, and it was necessary to specify the levels in the original units for each component.

$$\text{Pb removal (\%)} = +18.41162 + 11.97579\ \text{pH} + 0.445153 \rightarrow \text{conc.} - 0.023907\ \text{dosage} + 0.124341 \rightarrow \text{pH} * \text{conc} - 0.000203 \rightarrow \text{pH} * \text{dosage} - 0.002730\ \text{conc} * \text{dose} - 0.617548\ \text{pH}^2 - 0.020847 \rightarrow \text{conc}^2 + 0.000085\ \text{dosage}^2. \quad (4)$$

Table 3. The analysis of variance of the response surface quadratic model.

Source	Sum of Squares	df	Mean Square	F-Value	*p*-Value	
Model	4750.91	9	527.88	57.05	<0.0001	Significant
A-pH	3905.61	1	3905.61	422.09	<0.0001	
B-conc.	6.7	1	6.7	0.7242	0.049	
C-dose	0.1463	1	0.1463	0.0158	0.9012	
AB	67.35	1	67.35	7.28	0.0138	
AC	0.2367	1	0.2367	0.0256	0.8745	
BC	144.25	1	144.25	15.59	0.0008	
A^2	532.71	1	532.71	57.57	<0.0001	
B^2	6.86	1	6.86	0.7412	0.3995	
C^2	132.45	1	132.45	14.31	0.0012	
Residual	185.06	20	9.25			
Lack of Fit	90.5	5	18.1	2.87	0.0516	Not significant
Pure Error	94.56	15	6.3			
Cor Total	4935.97	29				

The three factors were subsequently optimized for maximum Pb removal from the simulated wastewater. The selection of the optimum conditions was based on the desirability functions. A desirability function assigns numerical values between 0 and 1 to each potential solution, where a value of 0 represents a fully unpleasant response and a value of 1 represents a perfectly desired or ideal response. As shown in Table 4, five solutions were selected based on desirability function of 1. However, solution 4 with the pH, initial Pb concentration, and catalyst dosage values of 10, 15 ppm, and 100 mg, respectively, was selected because a maximum Pb removal of 91.212% could be achieved. As shown in Table 5 and Figure 7, the RSM quadratic model was robust in fitting the experimental data since the predicted and the actual Pb ion removal rates were highly correlated. It can be seen that the data in Table 5 do not contain any outliers, as indicated by the internal studentized residuals. The benefit of internally and externally studentized residuals is that they make it simple to spot outliers by expressing the residuals' sizes in standard deviation units. Typically, an observation is considered an outlier if its internally and externally studentized residuals are more than 3 (in absolute value). A measure of a datapoint's effect is called a Cook's Distance. It considers the residual and the leverage of every observation. The amount that a regression model changes when the i-th observation is eliminated is summarized by a Cook's Distance. It can be seen that the effect of the Cook's Distance was minimized. The DFFITS statistic is a standardized measure of the change in the projected value for a specific observation when that observation is removed from an analysis. A high value suggests that the observation has a significant impact within its local area in the X space. High values of DFFITS suggest observations that have significant impacts on the results. A commonly used threshold is 2.

Table 4. Solution obtained from the RSM optimization.

Number	pH	Conc	Dosage	Pb Removal	Desirability
1	7.448	12.029	103.783	81.696	1
2	10	4	100	79.997	1

Table 4. *Cont.*

Number	pH	Conc	Dosage	Pb Removal	Desirability	
3	10	15	500	84.787	1	
4	10	15	100	91.212	1	Selected
5	7	9.5	300	74.844	1	

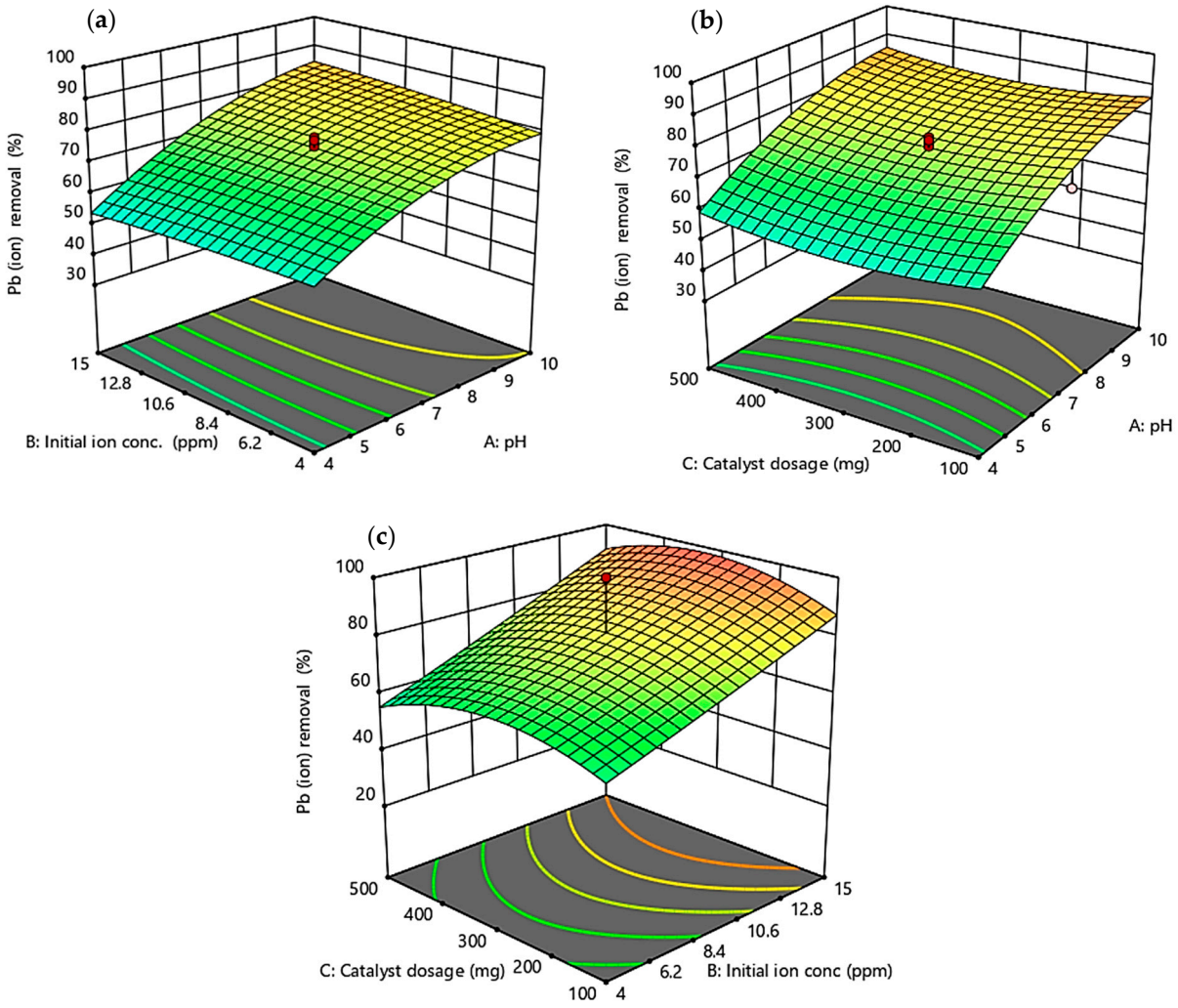

Figure 6. Effects of the interactions between (**a**) the initial ion concentration and pH, (**b**) the catalyst dosage and pH, and (**c**) the catalyst dosage and initial ion concentration.

Table 5. Comparison between the actual and the predicted Pb removal rates from the simulated wastewater.

Run Order	Actual Value	Predicted Value	Residual	Leverage	Internally Studentized Residuals	Externally Studentized Residuals	Cook's Distance	Influence on Fitted Value DFFITS	Standard Order
1	63.45	63.23	0.2272	0.371	0.094	0.092	0.001	0.07	5
2	72.34	78.32	−5.98	0.189	−2.181	−2.435	0.111	−1.174	21
3	36.23	35.47	0.7565	0.536	0.365	0.357	0.015	0.384	17
4	82.12	80	2.13	0.391	0.896	0.891	0.052	0.714	10
5	55.34	57.15	−1.81	0.391	−0.763	−0.755	0.037	−0.605	9
6	88.21	84.79	3.42	0.371	1.419	1.458	0.119	1.12	8
7	83.23	80	3.23	0.391	1.363	1.394	0.119	1.118	2
8	75.23	74.84	0.3904	0.119	0.137	0.133	0	0.049	27

Table 5. *Cont.*

Run Order	Actual Value	Predicted Value	Residual	Leverage	Internally Studentized Residuals	Externally Studentized Residuals	Cook's Distance	Influence on Fitted Value DFFITS	Standard Order
9	86.23	84.7	1.53	0.615	0.81	0.803	0.105	1.014	22
10	71.13	74.84	−3.71	0.119	−1.3	−1.324	0.023	−0.487	26
11	73.13	74.84	−1.71	0.119	−0.6	−0.59	0.005	−0.217	24
12	74.21	74.84	−0.6326	0.119	−0.222	−0.216	0.001	−0.08	23
13	94.23	91.21	3.02	0.391	1.272	1.293	0.104	1.036	4
14	76.32	74.84	1.48	0.119	0.518	0.508	0.004	0.187	25
15	75.23	73.93	1.3	0.536	0.629	0.619	0.046	0.666	20
16	52.23	54.22	−1.99	0.371	−0.826	−0.819	0.04	−0.629	15
17	65.34	63.23	2.12	0.371	0.878	0.873	0.045	0.67	13
18	78.23	74.84	3.39	0.119	1.187	1.2	0.019	0.442	29
19	86.21	91.21	−5	0.391	−2.107	−2.328	0.285	−1.866	12
20	83.24	84.79	−1.55	0.371	−0.641	−0.631	0.024	−0.485	16
21	77.23	74.84	2.39	0.119	0.836	0.83	0.009	0.305	28
22	80.12	81.37	−1.25	0.536	−0.603	−0.593	0.042	−0.638	18
23	57.45	57.15	0.2992	0.391	0.126	0.123	0.001	0.099	1
24	70.23	72.03	−1.8	0.536	−0.867	−0.861	0.087	−0.927	19
25	84.23	85.58	−1.35	0.371	−0.56	−0.55	0.019	−0.423	6
26	63.26	60.16	3.09	0.391	1.304	1.328	0.109	1.065	11
27	84.13	85.58	−1.45	0.371	−0.601	−0.591	0.021	−0.454	14
28	77.23	74.84	2.39	0.119	0.836	0.83	0.009	0.305	30
29	60.23	60.16	0.0722	0.391	0.03	0.03	0	0.024	3
30	51.22	54.22	−3	0.371	−1.244	−1.263	0.091	−0.97	7

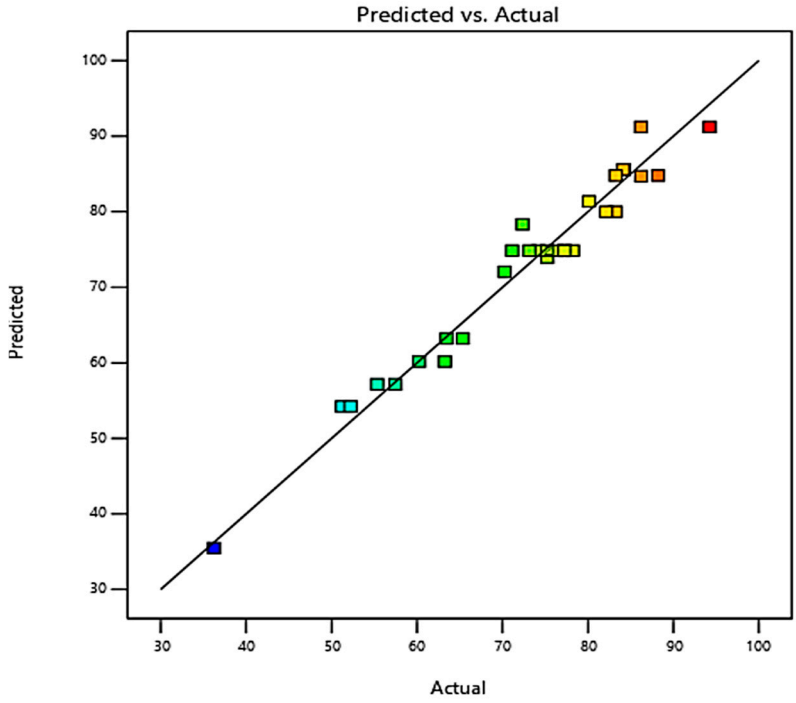

Figure 7. Comparison between the actual and the predicted Pb ion removal rates from the RSM quadratic model.

3.5. The Mechanism of Pb Removal from Wastewater

The process of the photocatalytic removal of Pb from wastewater using ZnO/ZrO_2 entails the generation of electrons and holes through the influence of light, followed by the adsorption of the Pb^{2+} ions. These ions are then reduced to a less soluble or metallic state and then eliminated from the aqueous phase. The ZnO/ZrO_2 composite is essential for optimizing the efficiency of this process by improving the charge separation and increasing the reactive surface area. When the ZnO/ZrO_2 photocatalyst is illuminated by visible light, it assimilates photons with energy that is equivalent to or beyond the bandgap

energy [46]. As a result of this stimulation, electrons (e^-) in the valence band are prompted to move to the conduction band, creating vacancies (holes) in the valence band, as shown by Equation (4). The Pb^{2+} ions adhere to the photocatalyst's surface by adsorption. The electrons produced by the action of light decrease the amount of Pb^{2+} ions that are adsorbed onto the surface, converting them into metallic Pb or a lower oxidation state (Equation (6)). This transformation causes the Pb to separate from the solution and form a precipitate.

$$ZnO/ZrO_2 + hv \rightarrow ZnO/ZrO_2\ \left(e^-_{CB} + h^+_{VB}\right), \text{ and} \quad (5)$$

$$Pb^{2+}_{ads} + 2e^-_{CB} \rightarrow Pb^o. \quad (6)$$

4. Conclusions

This work effectively utilized response surface methodology (RSM) to enhance the process of removing lead (Pb) from wastewater using ZnO/ZrO_2 composites by photocatalysis. The ZnO/ZrO_2 composite, when exposed to visible light, displayed effective photocatalytic activity, indicating its suitability for environmental remediation purposes. A systematic investigation was conducted on the impacts of important process factors on the efficiency of removing the Pb using a central composite design (CCD). The results of our study showed that the most effective circumstances for removing Pb (with a removal rate surpassing 90%) were obtained when using a dose of 100 mg/L of ZnO/ZrO_2, maintaining a pH of 10, and starting with an initial Pb content of 15 ppm. The response surface quadratic models precisely predicted the effectiveness of the Pb removal within the experimental domain, demonstrating the strength and dependability of the optimization strategy. The validation studies verified the efficacy of the adjusted settings, highlighting the practical use of RSM in improving photocatalytic processes for wastewater treatment. The combined impacts of ZnO and ZrO_2 in the composite were essential for increasing the photocatalytic activity, resulting in enhanced efficiency in degrading the Pb. In summary, this work provides important knowledge on improving the efficiency of removing Pb by photocatalysis utilizing ZnO/ZrO_2 composites with the use of RSM. The proposed optimal conditions may be used as a foundation for designing and scaling-up efficient photocatalytic systems for the removal of heavy metals in wastewater treatment facilities. Promising areas for future research involve delving deeper into the process by which Pb breaks down on ZnO/ZrO_2 surfaces, refining the methods used to synthesize the catalysts in order to improve their effectiveness, and carrying out extended studies to assess the long-lasting viability and practical usefulness of the optimized conditions in actual wastewater treatment scenarios. Overall, the combination of RSM with ZnO/ZrO_2 photocatalysts shows great potential in efficiently and sustainably eliminating Pb from wastewater. This progress in green technology contributes to the preservation of the environment and human health.

Author Contributions: Conceptualization, H.A.S. and M.A.A.; methodology, H.A.S. and M.A.A.; software, M.A.A.; validation, H.A.S., M.A.A. and A.K.M.; formal analysis, H.A.S.; investigation, H.A.S.; resources, M.A.A.; data curation, H.A.S.; writing—original draft preparation, H.A.S.; writing—review and editing, M.A.A. and A.K.M.; visualization, M.A.A.G.; supervision, M.A.A.; project administration, M.A.A.; Data curation and Visualization, K.A.S. All authors have read and agreed to the published version of the manuscript.

Funding: This research received no external funding.

Data Availability Statement: The data used are included in the manuscript.

Acknowledgments: The authors acknowledge the support of the Department of Chemical Engineering, University of Technology, Iraq.

Conflicts of Interest: The authors declare no conflicts of interest.

References

1. Ray, S.; Vashishth, R. From Water to Plate: Reviewing the Bioaccumulation of Heavy Metals in Fish and Unraveling Human Health Risks in the Food Chain. *Emerg. Contam.* **2024**, *10*, 100358. [CrossRef]
2. Sable, H.; Singh, V.; Kumar, V.; Roy, A.; Pandit, S.; Kaur, K.; Rustagi, S.; Malik, S. Toxicological and bioremediation profiling of nonessential heavy metals (mercury, chromium, cadmium, aluminium) and their impact on human health: A review. *Toxicol. Anal. Clin.* **2024**, *in press*. [CrossRef]
3. Alsaffar, M.A.; Ghany, M.A.R.A.; Mageed, A.K.; AbdulRazak, A.A.; Ali, J.M.; Sukkar, K.A.; Ayodele, B.V. Effect of Textural Properties on the Degradation of Bisphenol from Industrial Wastewater Effluent in a Photocatalytic Reactor: A Modeling Approach. *Appl. Sci.* **2023**, *13*, 8966. [CrossRef]
4. Raj, K.; Das, A.P. Lead pollution: Impact on environment and human health and approach for a sustainable solution. *Environ. Chem. Ecotoxicol.* **2023**, *5*, 79–85. [CrossRef]
5. Dave, D.M.; Yang, M. Lead in drinking water and birth outcomes: A tale of two water treatment plants. *J. Health Econ.* **2022**, *84*, 102644. [CrossRef] [PubMed]
6. Alsaedi, S.S.; Mohammed, S.S.; Mahdi, A.E.; Shnain, Z.Y.; Sh Majdi, H.; AbdulRazak, A.A.; Alwasiti, A.A. Modeling spinel oxide based-photocatalytic degradation of organic pollutants from industrial wastewater. *Chem. Eng. Commun.* **2024**, *211*, 603–613. [CrossRef]
7. Kumar, V.; Dwivedi, S.K.; Oh, S. A critical review on lead removal from industrial wastewater: Recent advances and future outlook. *J. Water Process. Eng.* **2022**, *45*, 102518. [CrossRef]
8. Ghorbani, M.; Seyedin, O.; Aghamohammadhassan, M. Adsorptive removal of lead (II) ion from water and wastewater media using carbon-based nanomaterials as unique sorbents: A review. *J. Environ. Manage* **2020**, *254*, 109814. [CrossRef] [PubMed]
9. Dhokpande, S.R.; Deshmukh, S.M.; Khandekar, A.; Sankhe, A. A review outlook on methods for removal of heavy metal ions from wastewater. *Sep. Purif. Technol.* **2024**, *350*, 127868. [CrossRef]
10. Fei, Y.; Hu, Y.H. Recent progress in removal of heavy metals from wastewater: A comprehensive review. *Chemosphere* **2023**, *335*, 139077. [CrossRef]
11. Mishra, S.; Sundaram, B. A review of the photocatalysis process used for wastewater treatment. *Mater. Today Proc.* **2023**, *in press*. [CrossRef]
12. Ali, H.M.; Arabpour Roghabadi, F.; Ahmadi, V. Solid-supported photocatalysts for wastewater treatment: Supports contribution in the photocatalysis process. *Sol. Energy* **2023**, *255*, 99–125. [CrossRef]
13. Lee, D.-E.; Kim, M.-K.; Danish, M.; Jo, W.-K. State-of-the-art review on photocatalysis for efficient wastewater treatment: Attractive approach in photocatalyst design and parameters affecting the photocatalytic degradation. *Catal. Commun.* **2023**, *183*, 106764. [CrossRef]
14. Hojjati-Najafabadi, A.; Farahbakhsh, E.; Gholamalian, G.; Feng, P.; Davar, F.; Aminabhavi, T.M.; Vasseghian, Y.; Kamyab, H.; Rahimi, H. Controllable synthesis of nanostructured flower-like cadmium sulfides for photocatalytic degradation of methyl orange under different light sources. *J. Water Process. Eng.* **2024**, *59*, 105002. [CrossRef]
15. Jabbar, Z.H.; Graimed, B.H.; Ammar, S.H.; Sabit, D.A.; Najim, A.A.; Radeef, A.Y.; Taher, A.G. The latest progress in the design and application of semiconductor photocatalysis systems for degradation of environmental pollutants in wastewater: Mechanism insight and theoretical calculations. *Mater. Sci. Semicond. Process.* **2024**, *173*, 108153. [CrossRef]
16. Ceretta, M.B.; Vieira, Y.; Wolski, E.A.; Foletto, E.L.; Silvestri, S. Biological degradation coupled to photocatalysis by ZnO/polypyrrole composite for the treatment of real textile wastewater. *J. Water Process. Eng.* **2020**, *35*, 101230. [CrossRef]
17. Jiad, M.M.; Abbar, A.H. Efficient wastewater treatment in petroleum refineries: Hybrid electro-fenton and photocatalysis (UV/ZnO) process. *Chem. Eng. Res. Des.* **2023**, *200*, 431–444. [CrossRef]
18. Wang, B.; Guo, Y.; Li, Q.; Xin, C.; Tian, Y.; Zhang, W.; Yu, X. Design of porous ZrO_2 with well-tuned band structures and strong visible-light harvesting via Zn doping for enhanced visible-light photocatalysis. *Chem. Eng. J.* **2024**, *481*, 148489. [CrossRef]
19. Gopal, V.; Harsha, S.; Selvaraj, A. Cow urine-based green synthesis of sunlight-responsive ZrO_2-Bi_2O_3 and its application in photocatalysis of 2,4-Dichlorophenoxyactetic acid in aqueous solution—Kinetics, mechanisms and sustainability analysis. *Catal. Commun.* **2024**, *187*, 106869. [CrossRef]
20. Maqbool, A.; Shahid, A.; Jahan, Z.; Niazi, M.B.K.; Inam, M.A.; Tawfeek, A.M.; Kamel, E.M.; Akhtar, M.S. Development of ZnO-GO-NiO membrane for removal of lead and cadmium heavy metal ions from wastewater. *Chemosphere* **2023**, *338*, 139622. [CrossRef]
21. Karthik, P.; Ravichandran, S.; Prakash, N.; Mukkannan, A.; Rajesh, J. Evaluation of ZnO infused CA/PCL nanocomposites using potential wastewater treatment and invitro anticancer activity. *Water Cycle* **2024**, *5*, 121–130. [CrossRef]
22. Geetha, M.; Vashisht, N.B.; Thanvir, S.; Roslan, N.C.; Mohamedzain, T.H.; Alfarwati, S.; Al-Lohedan, H.; Rajabathar, J.R.; Zaidi, S.A.; Sadasivuni, K.K. Multi-functional nanoscale ZrO_2 catalysts for sustainable water treatment. *Mater. Chem. Phys.* **2024**, *316*, 129096. [CrossRef]
23. Wahba, M.A.; Yakout, S.M.; Mohamed, W.A.A.; Galal, H.R. Remarkable photocatalytic activity of Zr doped ZnO and ZrO_2/ZnO nanocomposites: Structural, morphological and photoluminescence properties. *Mater. Chem. Phys.* **2020**, *256*, 123754. [CrossRef]
24. Majhool, A.K.; Sukkar, K.A.; Alsaffar, M.A. Combining α-Al2O3 Packing Material and a ZnO Nanocatalyst in an Ozonized Bubble Column Reactor to Increase the Phenol Degradation from Wastewater. *Processes* **2023**, *11*, 2416. [CrossRef]

25. Majhool, A.K.; Sukkar, K.A.; Alsaffar, M.A.; Majdi, H.S. Integrated Process for High Phenol Removal from Wastewater Employing a ZnO Nanocatalyst in an Ozonation Reaction in a Packed Bubble Column Reactor. *ChemEngineering* **2023**, *7*, 112. [CrossRef]
26. Ibrahim, M.M. Photocatalytic activity of nanostructured ZnO–ZrO_2 binary oxide using fluorometric method. *Spectrochim. Acta A Mol. Biomol. Spectrosc.* **2015**, *145*, 487–492. [CrossRef] [PubMed]
27. Ahmed, F.S.; Alsaffar, M.A.; AbdulRazak, A.A. One-step synthesis of magnetic fly ash composites for methylene blue removal: Batch and column study. *Environ. Sci. Pollut. Res.* **2023**, *30*, 124748–124766. [CrossRef] [PubMed]
28. Reza, A.; Chen, L.; Mao, X. Response surface methodology for process optimization in livestock wastewater treatment: A review. *Heliyon* **2024**, *10*, e30326. [CrossRef] [PubMed]
29. Bezerra, M.A.; Santelli, R.E.; Oliveira, E.P.; Villar, L.S.; Escaleira, L.A. Response surface methodology (RSM) as a tool for optimization in analytical chemistry. *Talanta* **2008**, *76*, 965–977. [CrossRef]
30. Ahmadi, A.; Heidarzadeh, S.; Mokhtari, A.R.; Darezereshki, E.; Harouni, H.A. Optimization of heavy metal removal from aqueous solutions by maghemite (γ-Fe_2O_3) nanoparticles using response surface methodology. *J. Geochem. Explor.* **2014**, *147*, 151–158. [CrossRef]
31. Maleki, S.; Karimi-Jashni, A.; Mousavifard, M. Removal of Ni(II) ions from wastewater by ion exchange resin: Process optimization using response surface methodology and ensemble machine learning techniques. *J. Environ. Chem. Eng.* **2024**, *12*, 112417. [CrossRef]
32. Tangahu, B.V.; Sheikh Abdullah, S.R.; Basri, H.; Idris, M.; Anuar, N.; Mukhlisin, M. Lead (Pb) removal from contaminated water using constructed wetland planted with Scirpus grossus: Optimization using response surface methodology (RSM) and assessment of rhizobacterial addition. *Chemosphere* **2022**, *291*, 132952. [CrossRef] [PubMed]
33. Patel, P.K.; Pandey, L.M.; Uppaluri, R.V.S. Adsorptive removal of Zn, Fe, and Pb from Zn dominant simulated industrial wastewater solution using polyvinyl alcohol grafted chitosan variant resins. *Chem. Eng. J.* **2023**, *459*, 141563. [CrossRef]
34. Biju, R.; Ravikumar, R.; Raghavan, J.R.V.; Indulal, C.R. Nanocomposite of zinc zirconia for better degradation of an organic dye. *Bull. Mater. Sci.* **2022**, *45*, 180. [CrossRef]
35. Alsaffar, M.A.; Rashid, S.A.; Ayodele, B.V.; Hamidon, M.N.; Yasin, F.M.; Ismail, I.; Hosseini, S.; Babadi, F.E. Response Surface Optimization of Multilayer Graphene Growth on Alumina-Supported Bimetallic Cobalt–Nickel Substrate. *Arab. J. Sci. Eng.* **2020**, *45*, 7455–7465. [CrossRef]
36. Pandey, J.; Shrivastava, V.; Nagarajan, R. Metastable $Bi_2Zr_2O_7$ with Pyrochlore-like Structure: Stabilization, Oxygen Ion Conductivity, and Catalytic Properties. *Inorg. Chem.* **2018**, *57*, 13667–13678. [CrossRef] [PubMed]
37. Aghabeygi, S.; Khademi-Shamami, M. ZnO/ZrO_2 nanocomposite: Sonosynthesis, characterization and its application for wastewater treatment. *Ultrason. Sonochem.* **2018**, *41*, 458–465. [CrossRef]
38. Khalili, S.; Chenari, H.M. The influence of ZrO_2 addition on the morphological, structural, vibrational, and optical characteristics of composite fibers based on ZnO. *Thin Solid Film.* **2022**, *741*, 139031. [CrossRef]
39. Haq, S.; Afsar, H.; Ali MBen Almalki, M.; Albogami, B.; Hedfi, A. Green Synthesis and Characterization of a ZnO-ZrO_2 Heterojunction for Environmental and Biological Applications. *Crystals* **2021**, *11*, 1502. [CrossRef]
40. Ban, T.; Sakai, T.; Ohya, Y. Synthesis of zinc oxide crystals with different shapes from zincate aqueous solutions stabilized with triethanolamine. *Cryst. Res. Technol.* **2007**, *42*, 849–855. [CrossRef]
41. Reddy, C.h.V.; Babu, B.; Reddy, I.N.; Shim, J. Synthesis and characterization of pure tetragonal ZrO_2 nanoparticles with enhanced photocatalytic activity. *Ceram. Int.* **2018**, *44*, 6940–6948. [CrossRef]
42. Ivanova, T.; Harizanova, A.; Koutzarova, T.; Vertruyen, B. Effect of annealing temperatures on properties of sol-gel grown ZnO-ZrO_2 films. *Cryst. Res. Technol.* **2010**, *45*, 1154–1160. [CrossRef]
43. Arote, S.A.; Pathan, A.S.; Hase, Y.V.; Bardapurkar, P.P.; Gapale, D.L.; Palve, B.M. Investigations on synthesis, characterization and humidity sensing properties of ZnO and ZnO-ZrO_2 composite nanoparticles prepared by ultrasonic assisted wet chemical method. *Ultrason. Sonochem.* **2019**, *55*, 313–321. [CrossRef]
44. Deepika, R.; Veerakumar, P. Microwave-assisted hydrothermal synthesis of ZnO@ZrO_2 nanohybrid for biomedical and photocatalytic applications. *Colloids Surf. A Physicochem. Eng. Asp.* **2024**, *688*, 133574. [CrossRef]
45. Fatimah, S.; Ragadhita, R.; Fitria, D.; Husaeni, A.; Bayu, A.; Nandiyanto, D. How to Calculate Crystallite Size from X-ray Diffraction (XRD) using Scherrer Method. *ASEAN J. Sci. Eng.* **2021**, *2*, 65–76. [CrossRef]
46. Priyadarshini, R.; Titus, A.; Sahoo, S.; Muppala, C.; Ramkumar, G.; Anh Pham, Q.; Rubavathy, S.J.; Rajasimman, M.; Hojjati-Najafabadi, A. Deep learning for the encounter of inorganic nanomaterial for efficient photochemical hydrogen production. *Int. J. Hydrogen Energy* **2024**, *52*, 664–673. [CrossRef]